ACS APPLIED MATERIALS & INTERFACES

Research Article

www.acsami.org

Hematite-Based Photoelectrochemical Water Splitting Supported by Inverse Opal Structures of Graphene

Ki-Yong Yoon,[†] Jung-Soo Lee,[†] Kwanghyun Kim,[†] Chang Hong Bak,[‡] Sun-I Kim,[†] Jin-Baek Kim,[‡] and Ji-Hyun Jang*,[†]

[†]School of Energy and Chemical Engineering, Low Dimensional Carbon Materials Center, Ulsan National Institute of Science and Technology (UNIST), Ulsan 689-798, Korea

[‡]Department of Chemistry, Korea Advanced Institute of Science and Technology (KAIST), Daejon 305-701, Korea

Supporting Information

ABSTRACT: By coupling α-Fe_2O_3 with a 3D graphene inverse opal (3D-GIO) conducting electrode, the short diffusion length of carriers and low absorption coefficient in α-Fe_2O_3 for photoelectrochemical applications were successfully addressed. GIO was directly grown on FTO substrate under low temperature conditions, removing the need for a graphene transfer process. α-Fe_2O_3 nanoparticles (NPs) were hydrothermally deposited on the surface of GIO, creating α-Fe_2O_3/GIO. The photocurrent density of α-Fe_2O_3/GIO in water splitting reactions reached 1.62 mA/cm^2 at 1.5 V vs RHE, which is 1.4 times greater than that of optimized α-Fe_2O_3. The EIS and IPCE data confirm reduced electron−hole recombination and fast electron transfer processes due to the short distance between active materials and the conducting electrode in the α-Fe_2O_3/GIO system. Our result may pave the way for designing devices in advanced energy conversion applications as well as a high efficiency hematite-based PEC system.

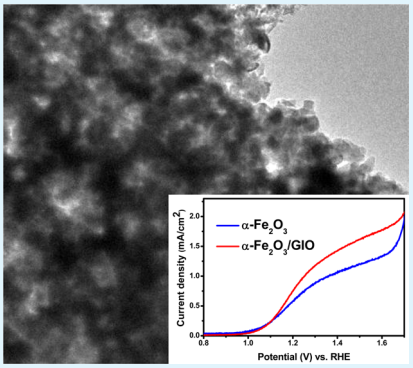

KEYWORDS: *water splitting , hydrogen generation, 3D graphene, short hole diffusion length, photoelectrochemical cells (PEC)*

Photoelectrochemical (PEC) water splitting utilizing semiconductors for solar hydrogen generation has received intense attention in the past decade.[1] Among many semiconductor materials, α-Fe_2O_3 is an earth-abundant, stable, and promising n-type candidate for solar water splitting with an appropriate bandgap of 2.2 eV, ranging in the visible region.[2−4] Three main issues remain to be addressed for cost-efficient α-Fe_2O_3 to be broadly used as a photoelectrode in PEC devices: its short hole diffusion length of 2−4 nm, which results in a high fraction of recombination; low absorption coefficient near the bandedge,[2] and the bulk/surface defects[5] that cause the high overpotential, low mobility of hole. Various efforts, such as nanostructuring,[6,7] impurity doping,[4] assembling a heterojunction,[8] and surface treating with Co-Pi or IrO_2,[9,10] have been suggested to overcome these issues in α-Fe_2O_3-based PEC devices. Another possible straightforward approach to address these drawbacks would be to directly and quickly transfer photogenerated electrons created in photoelectrodes to a 3D nanostructured current collector with photon trapping effects.

A three-dimensional (3D) nanonetwork is of considerable interest as an electrode material in energy-related areas because of its large surface area permitting a large number of accessible active sites, short-distance contact, and bicontinuity facilitating the transport of carriers.[11−14] As a conducting electrode, graphene has great potential because of its great electron mobility, transparency, and flexibility. Previous studies have tried to improve photocatalytic activity by the incorporation of graphene with good conductivity as well as catalytic properties.[15,16] However, most studies showed a relatively small increase in photocatalytic activity by using chemically synthesized graphene sheet. Among numerous techniques available for the preparation of graphene, chemical vapor deposition (CVD) growth of graphene on a metal or silica-coated silicon substrate is presently a powerful way to fabricate high quality and large area of graphene.[17−19] However, limitations caused by the high-temperature CVD growth condition, around 1000 °C, influence the choice of substrates, which might greatly determine the performance of the devices. For example, FTO glass, commonly used as a conducting substrate, has been questioned as a substrate for graphene growth, because it is unstable at high-temperature conditions because of the low melting temperature of the glass and the thin film of FTO. Thus, finding a way to grow graphene directly on the substrate, which removes the need for the transfer process, would bring great advantage for the broad and practical use of graphene.

In this work, we report a new type of 3D graphene conducting electrode which is directly grown on FTO substrate at 500 °C via carbon segregation on the surface of a 3D Ni inverse opal (NIO) frame. α-Fe_2O_3 NPs were decorated onto 3D graphene inverse opal (GIO) nanostructures via hydro-

Received: October 1, 2014
Accepted: November 21, 2014
Published: November 21, 2014

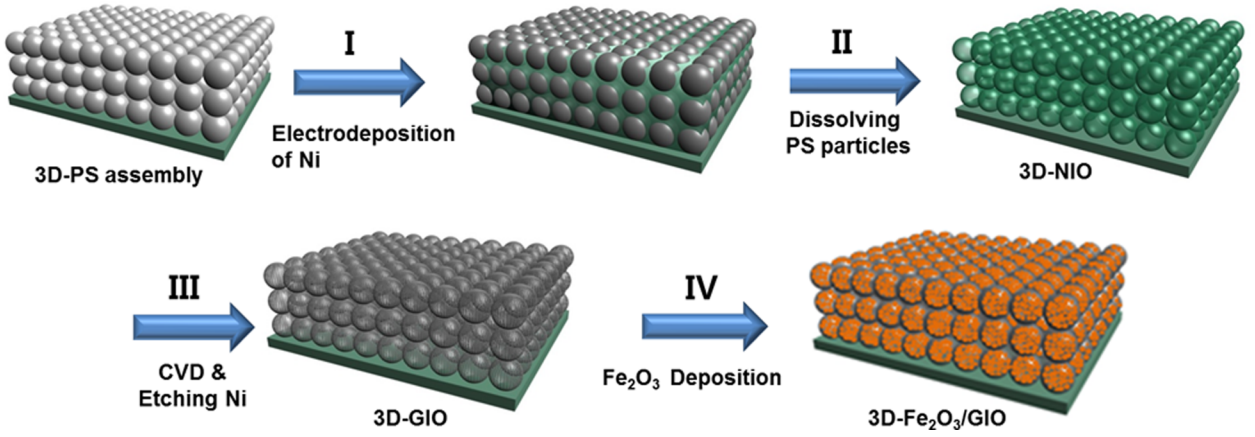

Figure 1. Illustration for the fabrication of α-Fe_2O_3/GIO.

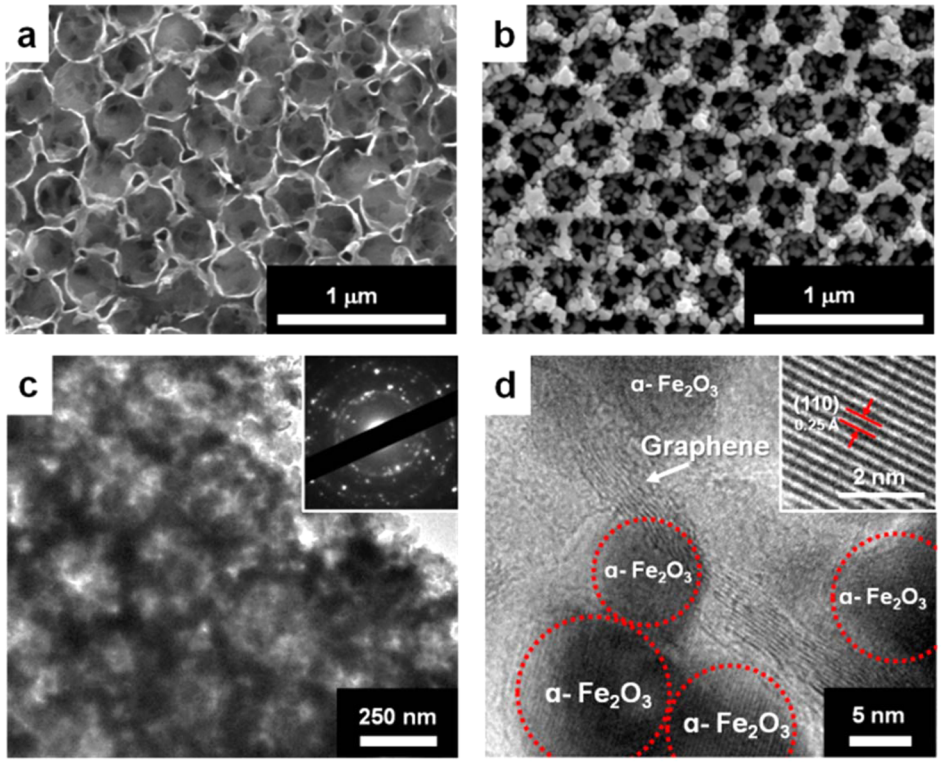

Figure 2. SEM images of (a) GIO after etching nickel and (b) α-Fe_2O_3/GIO. (c, d) TEM images of α-Fe_2O_3/GIO. The inset images in c and d are the SAED pattern and (110) lattice plane of α-Fe_2O_3, respectively.

thermal method for efficient water splitting reactions. The 3D-nanostructured α-Fe_2O_3/GIO exhibited 1.4 times increased efficiency relative to pristine α-Fe_2O_3 at a bias of 1.5 V, which can be attributed to the direct transfer of photogenerated electrons from α-Fe_2O_3 to the 3D graphene conducting electrode by short and direct contact.

α-Fe_2O_3/GIO was prepared by the following four steps, as illustrated in Figure 1. First, PS particles (350 nm) synthesized via emulsion polymerization were assembled into 3D opal structures on an FTO substrate, followed by electrodeposition of nickel onto the 3D opal structures (see Figure S1 in the Supporting Information). The dimension of PS was determined so as to efficiently scatter light for maximized light trapping as optimized in our previous reports.[20] Second, the PS opal structure was dissolved in toluene, leaving the nickel inverse opal (NIO) structures. Third, the prepared NIO was carburized using polyol solution at 250 °C with the assistance of catalytic Ni.[17] During the subsequent CVD process at 500 °C for 1 h under an Ar atmosphere, dissociated carbon percolated down through the NIO structures. The Raman spectra of GIO grown at various temperatures are shown in Figure S5 in the Supporting Information. The carbon then segregated from the carbon-dissolved NIO during the cooling processes, creating a graphene structure on the surface of the 3D NIO frame. After removing NIO, a 3D GIO with a diameter of 350 nm was created. Fourth, high crystalline α-Fe_2O_3/GIO was obtained by further heating the FeOOH NPs/GIO in two steps (350 °C, air and 750 °C, Ar, The conductivity of FTO treated under this condition is given in Table S2 in the Supporting Information). The annealing temperature of 750 °C was optimized for the samples to have the best crystalline nature as shown in Figure S6 in the Supporting Information.

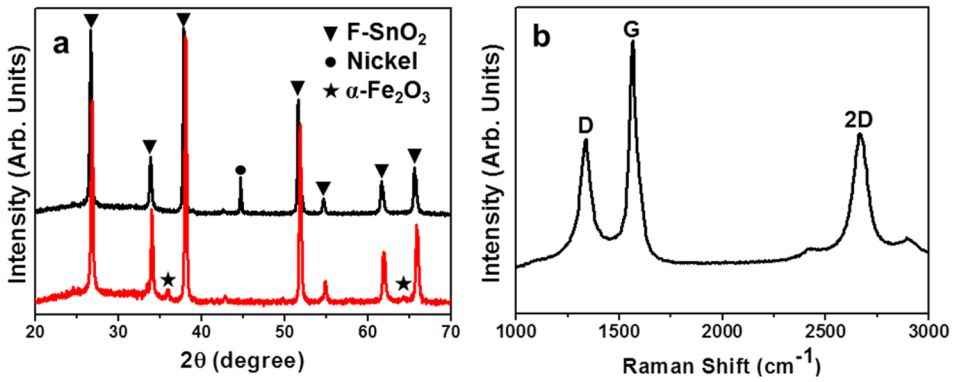

Figure 3. (a) XRD analysis of NIO (black line) and α-Fe_2O_3/GIO (red line) on FTO substrate. (b) Raman spectrum of GIO.

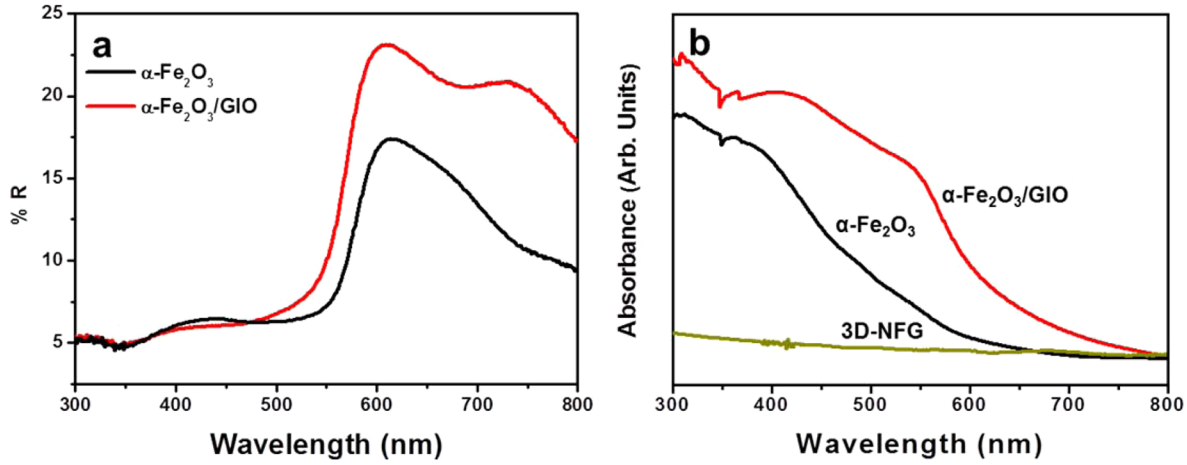

Figure 4. Optical properties of α-Fe_2O_3/GIO. (a) Diffuse reflectance spectra. (b) UV−visible spectra.

Figure 2a displays a scanning electron microscope (SEM) image of GIO. Because of the high carbon solubility of Ni, multilayer graphene was created, which agrees with the results of other related studies.[18] It should be noted that the GIO nanostructures were not considerably deformed and physicochemical properties of our low temperature-grown GIO, such as conductivity (1.4 kΩ/□) and transparency (59% at 550 nm), were not greatly inferior to those of graphene grown at 1,000 °C. A SEM image of α-Fe_2O_3 decorated on GIO is shown in Figure 2b (the elemental mapping data are shown in Figure S2 in the Supporting Information). Here, we targeted α-Fe_2O_3 NPs with diameters of less than 10 nm, which ensure a short diffusion path of holes to the surface of hematite, as well as enhanced surface area to compensate the relatively low number of active sites in the larger dimension GIO frame. The surface area was measured with 0.2 and 0.5 g of GIO and α-Fe_2O_3/GIO, respectively, by nitrogen adsorption−desorption isotherms. A plot of relative pressure vs volume absorbed was obtained by measuring the amount of N_2 gas that adsorbs onto the surface of interest and the subsequent amount that desorbs at a constant temperature (70 K). The surface area of α-Fe_2O_3/GIO was enhanced up to 63 m^2/g after α-Fe_2O_3 deposition, which is four times greater than 15 m^2/g of GIO (see Figure S4 in the Supporting Information). The details for controlling the size of FeOOH precursor NPs can be found in Figure S3 in the Supporting Information. The well-arranged pores in Figure 2b confirm α-Fe_2O_3/GIO maintains the original IO structures without great deformation. The transmission electron microscopy (TEM) images in Figure 2c, d reveal high density α-Fe_2O_3 nanoparticles with diameters of about 10 nm on the surface of ∼10 layers of graphene in α-Fe_2O_3/GIO. The selected area electron diffraction (SAED) patterns of α-Fe_2O_3 nanoparticles in the inset of Figure 2c are overlapped with the graphene pattern, implying the deposition of α-Fe_2O_3 nanoparticles onto GIO had occurred. The inset in Figure 2d shows the zoomed-up image of highly crystalline α-Fe_2O_3 particles with lattice spacing of 2.5 Å, corresponding to the (110) plane.

The formation of GIO and α-Fe_2O_3 NPs on the surface of GIO was confirmed by XRD and Raman analysis. The three peaks of α-Fe_2O_3 at 33.5, 35.92, and 64.3°, corresponding to the (104), (110) and (300) planes (JCPDS 99−000−1511) appeared in the XRD of α-Fe_2O_3/GIO.[21] The hematite obtained by a single step annealing process at 750 °C in an Ar atmosphere resulted in the creation of a mixture of Fe_2O_3 and Fe_3O_4 as shown in Figure S8 in the Supporting Information. The typical graphene peak at 26° corresponding to the (002) plane, which was created on the surface of NIO by CVD at 500 °C, was not detected in the XRD curve due to the overlap with the strong peak of FTO at 27°. Instead, the creation of graphene was proved by Raman data. Raman spectrum of GIO in Figure 3b revealed the D and G bands at around 1350, 1580, and the 2D band at 2700 cm^{-1} of graphene. The clear appearance of these main peaks, I_D/I_G ratio of 0.615, and I_{2D}/I_G ratio of 0.880 prove the creation of a multilayer of graphene, obtained under the low-temperature graphene growth conditions (500 °C). The Raman analysis of α-Fe_2O_3/GIO is shown in Figure S9 in the Supporting Information.

dx.doi.org/10.1021/am506721a | ACS Appl. Mater. Interfaces 2014, 6, 22634−22639

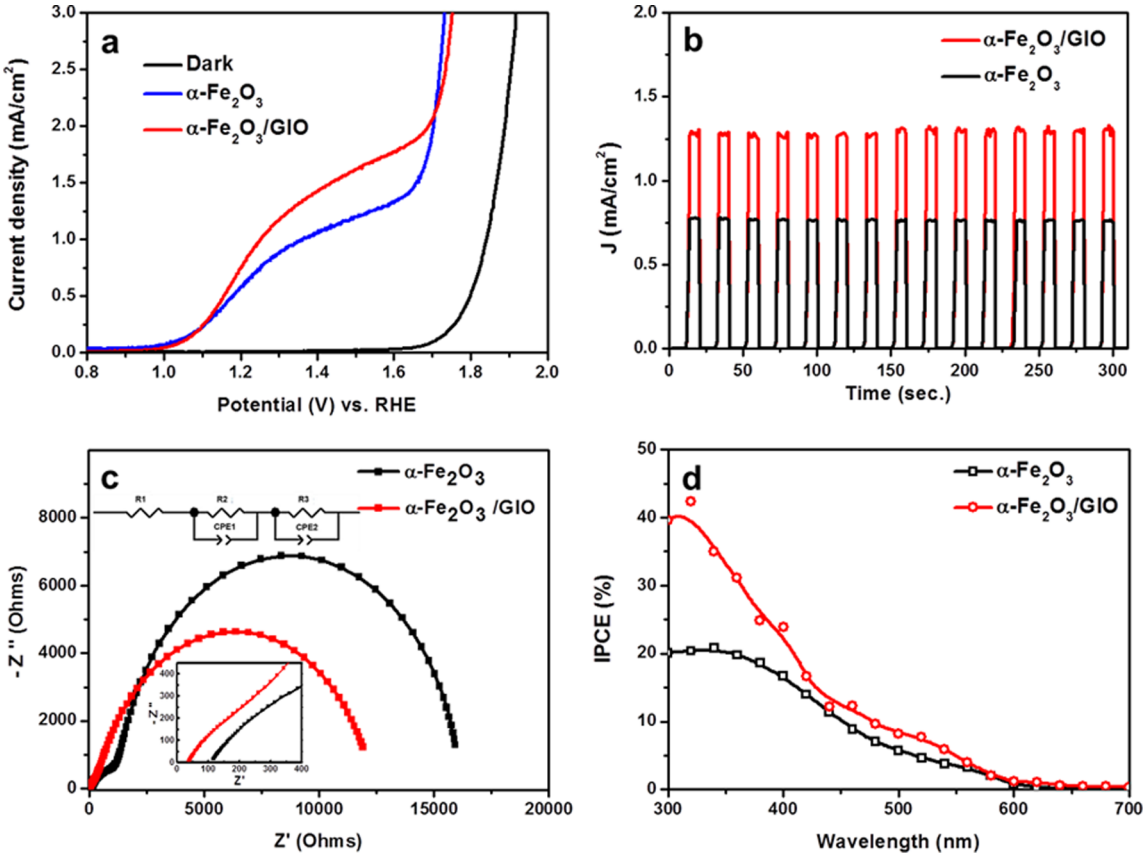

Figure 5. Photocurrent behaviors of α-Fe_2O_3/GIO. (a) Photocurrent vs potential of α-Fe_2O_3 and α-Fe_2O_3/GIO under UV−visible and dark conditions. (b) J−t curve of α-Fe_2O_3/GIO at a bias of 1.5 V vs RHE under UV−visible light illumination. (c) Nyquist plots and (d) IPCE of α-Fe_2O_3 and α-Fe_2O_3/GIO at a bias of 0.5 V vs open circuit potential under illumination.

We hypothesized that the GIO structures effectively provide a light-harvesting mechanism, which potentially improves the photoconversion efficiency of low absorptive α-Fe_2O_3 where it is poor, in the red spectral region, as reported in other IO-focused research.[22] To investigate the intensity of scattered light under beam irradiation, we measured the diffuse reflectance spectra of α-Fe_2O_3/GIO and α-Fe_2O_3, as shown in Figure 4a. Here, α-Fe_2O_3 is a nanostructured control sample with a thickness of 150 nm composed of NPs fabricated by the same method as the ones deposited on the surface of GIO. Compared to α-Fe_2O_3, the α-Fe_2O_3/GIO exhibited significantly higher diffuse reflection spectra in the visible spectrum of light (550−800 nm), indicating that the absorbed light was efficiently scattered within the nanostructure because of the dimensions of GIO in the few hundred nanometer scale, thus providing longer passages of light. The effect of introducing photon trapping GIO into the hematite was clearly observed by comparing the UV-extinction spectrum of the α-Fe_2O_3/GIO with two types of samples without the photon trapping effects, which were due to the small dimensions of the pores (the pristine α-Fe_2O_3 and graphene nanofoam containing ∼40 nm pores) as shown in Figure 4b. Compared to the typical absorption spectrum of the α-Fe_2O_3 and that of the 150 nm thick graphene nanofoam, which shows similar absorption peak values in the overall spectral range,[18] the α-Fe_2O_3/GIO showed a greatly raised characteristic absorption spectrum in the longer wavelength region (450−650 nm). This indicates that low absorption in α-Fe_2O_3 NPs was effectively overcome in α-Fe_2O_3/GIO, which can be attributed to GIO frame with the photon trapping effects (see the Tauc plot which shows a band gap of α-Fe_2O_3/GIO and α-Fe_2O_3 in Figure S11 in the Supporting Information).[23]

The photocurrent densities of α-Fe_2O_3/GIO were measured at a potential range from 0.6 to 2.0 V under AM 1.5 G simulated sunlight illumination, as shown in Figure 5a. Compared to pristine α-Fe_2O_3, the photocurrent density of α-Fe_2O_3/GIO exhibited great enhancement. The pristine α-Fe_2O_3 showed a photocurrent density of 1.17 mA/cm^2 at a bias of 1.5 V vs RHE, which is similar to the reported values of pristine α-Fe_2O_3 in other studies.[24] The maximum photocurrent density of α-Fe_2O_3/GIO reached 1.62 mA/cm^2 at 1.5 V vs RHE, which is 1.4 times higher than that of pristine α-Fe_2O_3. This increment can be attributed to the direct contact of α-Fe_2O_3 NPs onto 3D-conducting GIO which facilitates fast electron transfer through the bicontinuous networks in α-Fe_2O_3/GIO. The I−t curve of α-Fe_2O_3/GIO was obtained by chopped illumination of AM 1.5 G at an interval of 10 s on/off for UV−visible light at 1.5 V (Figure 5b). The abrupt occurrence and decay in the photocurrent density during the on/off illumination sequence implies the fast conduction of photocreated electrons from α-Fe_2O_3 to GIO. In order to explore the electrical behavior of α-Fe_2O_3 and α-Fe_2O_3/GIO, EIS measurements were carried out at a frequency range from 100 kHz to 0.1 Hz under 1 M NaOH electrolyte and open circuit voltage conditions (Figure 5c). The onset point on the real axis (R_s) at the high-frequency region represents the intrinsic resistance and the contact resistance of the electrode material with the substrate. The diameter of the semicircle, R_{ct},

at the middle frequency region conveys the interfacial charge transfer resistance. α-Fe_2O_3/GIO had a lower R_s value, of 36 Ω, than that of pristine α-Fe_2O_3, 109 Ω, indicating that the α-Fe_2O_3/GIO electrode has lower contact resistance and better intrinsic conductivity than the pristine α-Fe_2O_3 electrode (the EIS analysis of the GIO electrode is shown in Figure S10 in the Supporting Information). This implies a strong advantage of the direct and short-distance contact of α-Fe_2O_3 with a 3D-networked graphene current collector. The improvement can also be attributed to our direct growth method of GIO on FTO substrate. The diameter of the semicircle of α-Fe_2O_3/GIO at the middle frequency range is much smaller than that of α-Fe_2O_3, implying that α-Fe_2O_3/GIO provides pathways for more effective charge transfer between electrolytes and electrodes and thus more suppressed recombination (see Figure S7 in the Supporting Information). In Figure 5d, the incident photon-to-electron conversion efficiency (IPCE) of Fe_2O_3/GIO exhibits a maximum value of 42% at 320 nm with an extended photoresponse window up to 600 nm and is overall much higher than that of a typical α-Fe_2O_3 electrode, indicating that more photons have been converted to currents in α-Fe_2O_3/GIO.

In conclusion, we have shown that by coupling GIO with photoelectrode materials, the problem of low diffusion length and low absorption in α-Fe_2O_3 was efficiently addressed, and thereby the water splitting photocurrent density generated by α-Fe_2O_3 could be greatly enhanced. GIO, directly grown on FTO substrate at low temperature conditions, provides the 3D conducting networks for shuttling electrons and photon trapping effects. The diffuse reflectance spectra and EIS data respectively proved the enhanced absorption, and the presence of direct and fast electron transfer pathways and reduced electron−hole recombination in α-Fe_3O_3/GIO showed 1.4 times higher PEC value than that of typical α-Fe_2O_3 at 1.5 V vs RHE. Furthermore, the preparation method and the methodology for the design introduced here can be readily extended to other metal oxide materials and systems, which provide strong potential for our strategy in energy conversion systems.

■ ASSOCIATED CONTENT

Ⓢ Supporting Information

Experimental details, SEM, XPS, BET, Raman, XRD, scheme, sheet resistance, EIS and Tauc plot analysis of the samples (α-Fe_2O_3 and α-Fe_2O_3/GIO). This material is available free of charge via the Internet at http://pubs.acs.org/.

■ AUTHOR INFORMATION

Corresponding Author

*E-mail: clau@unist.ac.kr.

Author Contributions

The experiments were performed by K.Y., J.L., K.K, and C.B. with suggestions from J.K and J.J.; K.Y. and J.L. prepared Fe_2O_3/GIO samples. K.K. performed PEC and electrochemical measurements. J.J. analyzed the data and wrote the manuscript. All authors discussed the results and commented on the manuscript

Notes

The authors declare no competing financial interest.

■ ACKNOWLEDGMENTS

This work is supported by NRF with the contract no. NRF-2010- 0019408 and 2014-M2B2A4030415 (National nuclear R&D program, MSIP) and by Ministry of Trade, Industry & Energy of Korea (10040038).

■ REFERENCES

(1) Fujishima, A.; Honda, K. Electrochemical Photolysis of Water at a Semiconductor Electrode. *Nature* **1972**, *238*, 37−38.

(2) Walter, M. G.; Warren, E. L.; McKone, J. R.; Boettcher, S. W.; Mi, Q.; Santori, E. A.; Lewis, N. S. Solar Water Splitting Cells. *Chem. Rev.* **2010**, *110*, 6446−6473.

(3) Sivula, K.; Le Formal, F.; Gratzel, M. Solar Water Splitting: Progress Using Hematite (α-Fe2O3) Photoelectrodes. *ChemSusChem* **2011**, *4*, 432−449.

(4) Kim, J. Y.; Magesh, G.; Youn, D. H.; Jang, J. W.; Kubota, J.; Domen, K.; Lee, J. S. Single-Crystalline, Wormlike Hematite Photoanodes for Efficient Solar Water Splitting. *Sci. Rep.* **2013**, *3*, 2681.

(5) Sanchez, C.; Sieber, K. D.; Somorjai, G. A. The Photoelectrochemistry of Niobium Doped Alpha-Fe2(03). *J. Electroanal. Chem.* **1988**, *252*, 269−290.

(6) Wheeler, D. A.; Wang, G.; Ling, Y.; Li, Y.; Zhang, J. Z. Nanostructured Hematite: Synthesis, Characterization, Charge Carrier Dynamics, and Photoelectrochemical Properties. *Energy Environ. Sci.* **2012**, *5*, 6682−6702.

(7) Ahn, H.-J.; Kwak, M.-J.; Lee, J.-S.; Yoon, K.-Y.; Jang, J.-H. Nanoporous Hematite Structures to overcome Short Diffusion Lengths in Water Splitting. *J. Mater. Chem. A* **2014**, *2*, 19999−20003.

(8) Hou, Y.; Zuo, F.; Dagg, A.; Feng, P. A Three-Dimensional Branched Cobalt-Doped α-Fe2O3 Nanorod/MgFe2O4 Heterojunction Array as a Flexible Photoanode for Efficient Photoelectrochemical Water Oxidation. *Angew. Chem., Int. Ed.* **2013**, *52*, 1248−1252.

(9) Klahr, B.; Gimenez, S.; Fabregat-Santiago, F.; Bisquert, J.; Hamann, T. W. Photoelectrochemical and Impedance Spectroscopic Investigation of Water Oxidation with "Co-Pi"-Coated Hematite Electrodes. *J. Am. Chem. Soc.* **2012**, *134*, 16693−16700.

(10) Tilley, S. D.; Cornuz, M.; Sivula, K.; Gratzel, M. Light-Induced Water Splitting with Hematite: Improved Nanostructure and Iridium Oxide Catalysis. *Angew. Chem., Int. Ed.* **2010**, *49*, 6405−6408.

(11) Halaoui, L. I.; Abrams, N. M.; Mallouk, T. E. Increasing the Conversion Efficiency of Dye-Sensitized TiO2 Photoelectrochemical Cells by Coupling to Photonic Crystals. *J. Phys. Chem. B* **2005**, *109*, 6334−6342.

(12) Chen, J. I. L.; von Freymann, G.; Choi, S. Y.; Kitaev, V.; Ozin, G. A. Slow Photons in The Fast Lane in Chemistry. *J. Mater. Chem.* **2008**, *18*, 369−373.

(13) Chen, X.; Ye, J.; Ouyang, S.; Kako, T.; Li, Z.; Zou, Z. Enhanced Incident Photon-to-Electron Conversion Efficiency of Tungsten Trioxide Photoanodes Based on 3D-Photonic Crystal Design. *ACS Nano* **2011**, *5*, 4310−4318.

(14) Nishimura, S.; Abrams, N.; Lewis, B. A.; Halaoui, L. I.; Mallouk, T. E.; Benkstein, K. D.; van de Lagemaat, J.; Frank, A. J. Standing Wave Enhancement of Red Absorbance and Photocurrent in Dye-Sensitized Titanium Dioxide Photoelectrodes Coupled to Photonic Crystals. *J. Am. Chem. Soc.* **2003**, *125*, 6306−6310.

(15) Zhang, H.; Lv, X. J.; Li, Y. M.; Wang, Y.; Li, J. H. P25-Graphene Composite as a High Performance Photocatalyst. *ACS Nano* **2010**, *4*, 380−386.

(16) Xiang, Q. J.; Yu, J. G.; Jaroniec, M. Synergetic Effect of MoS2 and Graphene as Cocatalysts for Enhanced Photocatalytic H-2 Production Activity of TiO2 Nanoparticles. *J. Am. Chem. Soc.* **2012**, *134*, 6575−6578.

(17) Yoon, S.-M.; Choi, W. M.; Baik, H.; Shin, H.-J.; Song, I.; Kwon, M.-S.; Bae, J. J.; Kim, H.; Lee, Y. H.; Choi, J.-Y. Synthesis of Multilayer Graphene Balls by Carbon Segregation from Nickel Nanoparticles. *ACS Nano* **2012**, *6*, 6803−6811.

(18) Lee, J.-S.; Ahn, H.-J.; Yoon, J.-C.; Jang, J.-H. Three-Dimensional Nano-Foam of Few-Layer Graphene Grown by CVD for DSSC. *Phys. Chem. Chem. Phys.* **2012**, *14*, 7938−7943.

(19) Yoon, J. C.; Lee, J. S.; Kim, S. I.; Kim, K. H.; Jang, J. H. Three-Dimensional Graphene Nano-Networks with High Quality and Mass

Production Capability via Precursor-Assisted Chemical Vapor Deposition. *Sci. Rep.* **2013**, *3*, 1788.
(20) Kim, K.; Thiyagarajan, P.; Ahn, H.-J.; Kim, S.-I.; Jang, J.-H. Optimization for Visible Light Photocatalytic Water Splitting: Gold-Coated and Surface-Textured TiO_2 Inverse Opal Nano-Networks. *Nanoscale* **2013**, *5*, 6254−6260.
(21) Nakau, T. Electrical Conductivity of a-Fe_2O_3. *J. Phys. Soc. Jpn.* **1960**, *15*, 727−727.
(22) Zhang, K.; Shi, X.; Kim, J. K.; Lee, J. S.; Park, J. H. Inverse Opal Structured [small alpha]-Fe_2O_3 on Graphene Thin Films: Enhanced Photo-Assisted Water Splitting. *Nanoscale* **2013**, *5*, 1939−1944.
(23) Sivula, K.; Zboril, R.; Le Formal, F.; Robert, R.; Weidenkaff, A.; Tucek, J.; Frydrych, J.; Gratzel, M. Photoelectrochemical Water Splitting with Mesoporous Hematite Prepared by a Solution-Based Colloidal Approach. *J. Am. Chem. Soc.* **2010**, *132*, 7436−7444.
(24) Shi, X.; Zhang, K.; Shin, K.; Moon, J. H.; Lee, T.-W.; Park, J. H. Constructing Inverse Opal Structured Hematite Photoanodes via Electrochemical Process and Their Application to Photoelectrochemical Water Splitting. *Phys. Chem. Chem. Phys.* **2013**, *15*, 11717−11722.